https://doi.org/10.5194/esd-2024-27
Preprint. Discussion started: 23 September 2024

Earth System Dynamics
Discussions

The visible and hidden climatic effects on Earth's denudation

Iván Vergara[1,2*], Fernanda Santibañez[3,4], René Garreaud[1,5], Germán Aguilar[6]

[1] Center for Climate and Resilience Research (CR)2, Chile
[2] IPATEC, CONICET-UNCo, Río Negro, Argentina
[3] National University of Río Negro, IRNAD, Río Negro, Argentina
[4] National Scientific and Technical Research Council, IRNAD, Río Negro, Argentina
[5] Department of Geophysics, University of Chile, Santiago, Chile
[6] Advanced Mining Technology Center, University of Chile, Santiago, Chile

Correspondence to: Ivan Vergara (ivergara@comahue-conicet.gob.ar)

Abstract. Denudation is the opposite process of mountain uplift and plays a major role in the Earth system. Despite the research to constrain its environmental control, uncertainties remain about which are the dominant physicochemical processes at play. Here, the ^{10}Be-derived denudation rate, encompassing time windows from 10^2 to 10^5 yr, was modelled in over a thousand basins across the Earth. The results suggest that water and associated life have a positive effect across their whole range, which is regulated by topography due to processes such as the energy expended by rivers on their beds, the feedback between erosion and weathering, and the transport and production rate of soils. Consequently, bioclimatic influence is weak in flat landscapes, but it could vary denudation forty times in mountain settings. It was also observed that other things being equal, water availability steepens basins, so climate also has an indirect effect acting on geological timeframes. The results can be useful for the landscape´s numerical modelling and highlight the importance of climate on denudation.

1 Introduction

The denudation –bedrock and sediment loss from the Earth's surface– mediates the effect that climate can have on tectonics (Whipple, 2009; Hu et al., 2021; Forte et al., 2022), together with uplift drives landscape evolution (Fischer et al., 2021), and directly and indirectly influences several human activities such as agriculture, hydroelectric energy production, fishing, and water storage and consumption (Masotti et al., 2018; Li et al., 2022; Vergara et al., 2022). The denudation comprises erosion –the mechanical component– and weathering –the chemical component–. Within the first component, the following processes can be highlighted: a) fluvial erosion, that depends mostly on channel slope, which is mainly generated by spatial variability of tectonic uplift (Seybold et al., 2021); b) landsliding, that is a function of slope, lithology, soil moisture and seismicity, and usually occur upon diffusive terrains known as hillslopes (Antinao and Gosse, 2009; Campforts et al., 2022); and c) glacial erosion, which depends on basal velocity and spatiotemporal variations in meltwater drainage, and in some Earth's periods was the main denudative process (Koppes, et al., 2015; Herman et al., 2021). On the other hand, weathering generally has positive feedback with erosion and also increases with rock solubility, temperature, water availability, and vegetation, which releases acids through roots (Hinderer et al., 2013; Perron, 2017; Porder, 2019).

The difficulty of measuring denudation and the multiple physicochemical processes involved led to most of the studies that quantified its environmental control being carried

https://doi.org/10.5194/esd-2024-27
Preprint. Discussion started: 23 September 2024

Earth System Dynamics
Discussions
Open Access

out at a regional dimension or having focused on specific processes. Regional studies generally do not include the full range of values that controlling variables have on the Earth, much less all the combinations of values existing between them. This can cause errors in detecting the true effects of forcing factors, and lead to multicollinearity in statistical approaches, which worsens the detection of the true effects (Vergara et al., 2023). On the other hand, concentrating on specific denudation processes generated important theoretical advances (Iverson, 2012; Roering, 2008), but it does not allow comparing the relative weight of each one and hinders the understanding of basins' total denudation where several processes usually coexist. These difficulties limit the knowledge about the combined control of endogenous and exogenous forces acting in different timeframes. Here, through statistical modelling it was identified the environmental variables that together best predict the denudation in ~1,700 highly diverse basins around the Earth, to infer later which are the dominant controlling processes behind (Fig. 1). Denudation was calculated from ^{10}Be concentration in present-day river sediment, which depends on the impact time of secondary cosmic rays on the surface's minerals and is precisely inversely proportional to the average denudation rate (m kyr^{-1}) of the upstream catchment for temporal windows from 10^2 to 10^5 yr (Codilean et al., 2022).

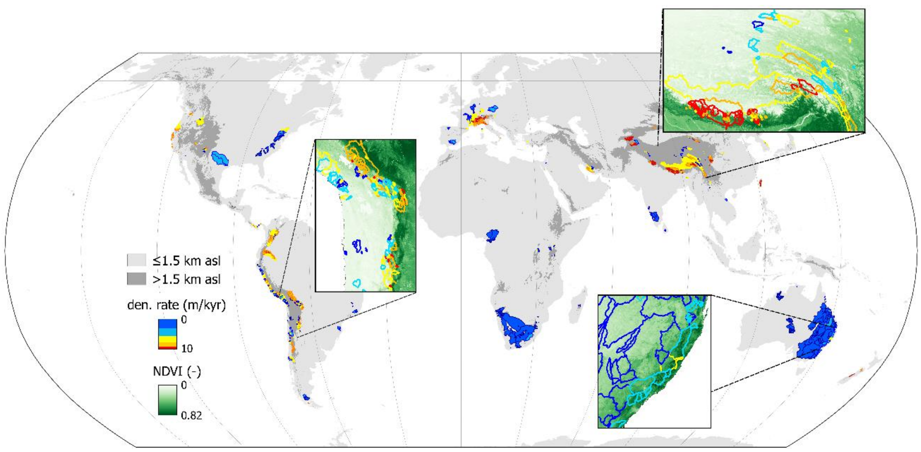

Figure 1: Location of the basins studied. Higher denudation can be seen on mountain ranges. Insets with NDVI maps are regions where climate effect on denudation is evident: Hymalayas with higher moisture southward and subtropical Andes and Great Dividing Range with higher moisture eastward (Codilean et al., 2021).

2 Results

The multiple regression chosen using the automatic model selection approach has an Adjusted R^2 of 78%, which would be the best physically plausible denudation prediction for a planetary scope so far (Portenga and Bierman, 2011; Willenbring et al., 2013; Mishra et al., 2019; Ruetenik et al., 2023) (Appendixes). The model includes the effects of terrain slope, seismicity, lithologic hardness, cryosphere development, and the first Principal Component between precipitation, soil moisture and vegetation development, referred as *clim*.

$$\mathrm{den} \propto (\mathrm{PGA}+1)^{0.8}\, e^{-0.004\mathrm{lit}+0.4\mathrm{cry}+3.2\mathrm{sl}+0.3\mathrm{clim}} \quad (1)$$

https://doi.org/10.5194/esd-2024-27
Preprint. Discussion started: 23 September 2024

Earth System Dynamics
Discussions

The predictively insignificant incorporation of the area as a covariate suggests that ^{10}Be enrichment related to travel time (Carretier et al., 2009) is irrelevant for most basins. Although seismicity and slope partly represent the same process, i.e., uplift, the model was allowed to include both because seismicity also expresses the fracturing of rock massifs and the triggering of landslides. The cryospheric effect includes an overestimation because sediment coming from bedrock underlying glaciers and seasonal snowpack is shielded from secondary cosmic rays and, therefore, does not represent a real denudation rate (Delunel et al., 2010). In this sense, the cryospheric covariate was used to quantify the denudative processes of this environment (Vergara et al., 2020; Zhang, et al., 2022) and to isolate the overestimation. As an alternative method to isolate that error, a new dataset was generated excluding basins with a plenty of solid precipitation or glacial volume, which gave analogous results (Table S1).

The model captures the multiplicative effect between topography and water availability that occurs on fluvial and soil erosion (Fig. 2a; see next section). However, analysis of the raw data shows that topography and climate effects not only multiply each other, but also increase their exponents (Fig. 2c,d). To include this phenomenon in the model, the explicit multiplication of both covariates was added as a factor, allowing their exponents to interact and improving the prediction by 1% (Figs. 2b & S1; Table S2).

$$\mathrm{den} \propto (\mathrm{PGA}+1)^{0.8}\, e^{-0.004\mathrm{lit}+0.4\mathrm{cry}+3.1\mathrm{sl}+0.1\mathrm{clim}+0.4\mathrm{sl\ clim}} \qquad (2)$$

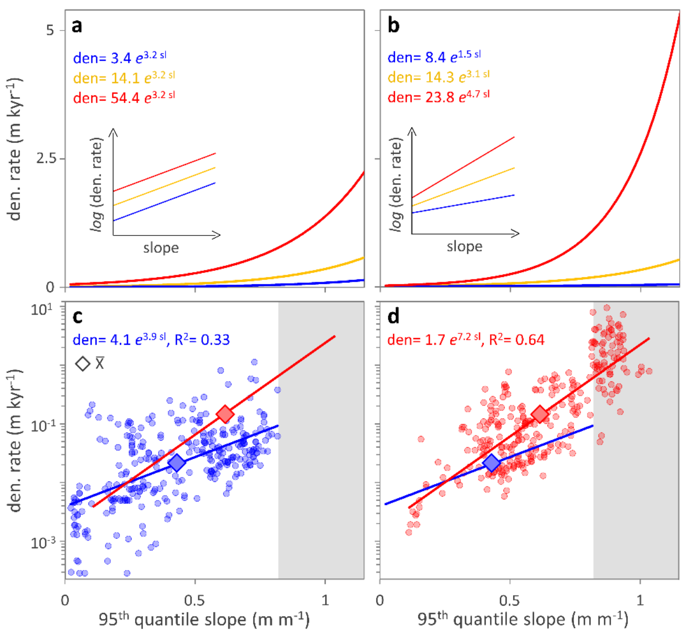

Figure 2: (*a*) Predicted denudation rate based on Eq. 1 as a function of slope and setting *clim* at its minimum (blue), average (orange) and maximum (red) and the other covariates at their averages. (b) Same as the previous panel but using Eq. 2. (*c, d*) Exponential regression between slope and denudation rate for the 300 basins without high solid precipitation and glacial development and with the lowest (blue) and highest (red) values of *clim*. Grey area indicates the x-axis interval without basins with the lowest *clim* values. Note that the generation of subgroups of different sizes gives analogous results (Table S3). Go to Fig. S2 to see the same plots, but with the roles of slope and *clim* reversed.

3 Discussion

The first aspect of the model to be discussed is the joint effect –hardly separable through statistics– of precipitation, soil moisture, and vegetation. Its positive sign –even though the ^{10}Be method underestimates weathering (Riebe and Granger, 2013)– (Fig. 2d) indicates that denudation-promoting mechanisms, such as soil surcharge and river energy (Ferrier et al., 2013), outweigh negative ones, such as runoff obstruction by vegetation or enlarged soil cohesion caused by root anchorage (Vergani et al., 2017; Schmid et al., 2018) (Sup. Material). Furthermore, positive sign of vegetation's factor loading in $PC1_{clim}$ suggests that vegetation resulting influence is positive for the analysed temporal windows. The bioclimatic effect is widely debated precisely due to its multiple influences with opposed directions that are difficult to address together through physically based models. It is widely agreed that precipitation has a positive effect from hyper-arid to semi-arid environments, but towards wetter settings where vegetation begins to rise markedly, it was measured from a continuation of the effect's direction (Marder and Gallen, 2023), as in this study, to one or more reversals (Vergara et al., 2023; Mishra et al., 2019; Langbein and Schumm, 1958; Walling and Kleo, 1979; DiBiase and Whipple 2011; Torres Acosta et al., 2015; Chen et al., 2022). Part of the disagreement may be because many studies do not include solute load, so runoff obstruction impact on clastic load is highlighted and weathering produced by water, roots and fungi is underestimated. In addition, these studies integrate annual to decadal timeframes that do not adequately capture the recurrence of mass transport events in vegetated mountains and, consequently, the high soil production there (Mohr et al., 2023).

Another point to deepen is that the selected model represents more the denudation generated on hillslope than that generated by river network. In selecting a topographic covariate (Appendices B and C), the slope of the entire basin enters before the stream power or its morphometric solution, i.e., the Normalized Channel Steepness Index (Smith et al., 2022). This also happens for bioclimatic variables where the first one associated with runoff or streamflow enters after six related to soil moisture, vegetation or mean precipitation (Table S14). In fact, if we force a selection of models in which only topographic and climatic variables related to fluvial dynamics can enter, the chosen model explains 9% less variance (Table S4). The higher predictivity of variables related to hillslope suggests that for most basins the majority of denuded mass comes from there. The long-term denudation rate of hillslopes can be equal to that of rivers under certain evolutionary conditions of basins (Ruetenik et al., 2023; Roering, 2012; Campforts et al., 2020), but it is lower when the complete history of basins is considered, a fact that is reflected in the lower elevation of rivers relative to the surrounding mountains despite the similar uplift. Therefore, the lower denuded mass produced by rivers would be because they cover a small proportion of landscape, which is between ~0 and 3% of the non-cryospheric surface of the basins studied (Sup. Material).

The final model includes a positive interaction between slope and *clim*, whereby the effect of each is progressively amplified through the coefficient and exponent as the other increases (Fig. 2a,d). The multiplication between the covariates partly determines: a) the erosion or transport of soil, which depends on the terrain gradient and biological disturbances such as root growth (Roering et al., 2008; Chen et al., 2014), and b) the energy that rivers expend on their beds and, collaterally, the erosion they generate (Appendix B). A third process that would imply a multiplicative effect of slope and climate is the rate of soil production, which depends on the product of its moisture and the negative exponential effect of its thickness (Heimsath et al., 1997; Amundson et al., 2015). Given that, all else being equal, the frequency of soil removal and thinning increases with slope, it is possible that the rate of soil production is reflected in equations 1 and 2. Instead, the increase in

https://doi.org/10.5194/esd-2024-27
Preprint. Discussion started: 23 September 2024

Earth System Dynamics
Discussions

exponents generated by the interaction between topography and climate may be related to the positive feedback between weathering -more associated with climate- and erosion -more associated with topography-, but further research is needed on this topic (West, 2012; Murphy et al., 2016).

The Figure 2c,d shows that the basin subgroups are separated along both axes, suggesting not only that bioclimatic condition has an influence on denudation –Δy–, but also that aridity may impose an upper limit on basin slopes –Δx–. Relating this possible limit with the interaction of Figure 2b, it is estimated that, for equal and natural conditions, the maximum variation that bioclimatic state can generate on denudation is 38^{+18}_{-12} times (≡ $1.1^{+0.2}_{-0.2}$ m kyr^{-1}) and not 109^{+108}_{-54}, which would be calculated by assuming the existence of extremely steep, arid basins. More importantly, the limit would indicate that a humid climate generates steeper catchments, possibly because greater water availability produces a denser drainage network with deeper and narrower river valleys (Rehak et al., 2010; Harries et al., 2023). This idea is confirmed by explaining 73% of variance of basins average slope through precipitation, lithology, cryosphere development, seismicity and elevation, so that, in addition to the direct climate effects described, there is an indirect one associated with denudation-promoting steepening (Fig. 3; Sup. Material; Table S6).

$$\mathrm{sl} \propto (\mathrm{lit}+1)^{-0.02}\,(\mathrm{PGA}+0.1)^{0.1}\,\mathrm{pp}^{0.2}\,(\mathrm{elev}+100)^{0.1}\,e^{0.1\mathrm{cry}} \quad (3)$$

The direct effects would act with a recurrence of up to a few hundreds or thousands of years, while landscape shaping would act in time windows of hundreds of thousands to millions of years. Finally, the similar complex relationship would occur in glacial erosion, where the effects of terrain slope and ice thickness, i.e., climate favourability, multiply (Cuffey and Paterson, 2010), and in turn, glacial erosion steepens terrain promoting further erosion (Fig. 3c).

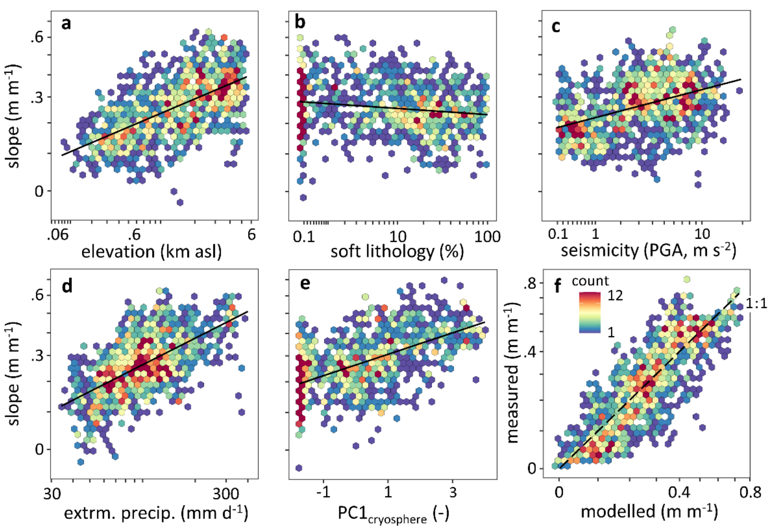

Figure 3: (*a*-e) Partial effects of each covariate in the regression model for the basins' average slope. Solid lines indicate predicted fits as a function of x-axis covariate and fixing the others at their averages. Similar relationships are obtained by predicting the 95th quantile of basin slopes (Table S7). (*f*) Measured vs. modelled slope.

https://doi.org/10.5194/esd-2024-27
Preprint. Discussion started: 23 September 2024

Earth System Dynamics
Discussions

The combination of direct and indirect effects operating at different time windows magnifies the role that climate spatiotemporal variability has on the Earth's denudation. The suitable prediction of denudation obtained allows it to be simulated for the rest of the Earth, to known, for example, the mass of sediments and nutrients exported to the sea. In turn, the better understanding of the environmental processes that control denudation could be useful to advance in the knowledge of the carbon cycle and to improve numerical models used to study landscape evolution (Chen et al., 2014; Barnhart et al., 2020).

Appendix A: Denudation rate

A global database of ^{10}Be-derived denudation rates (m kyr^{-1}) in 4,290 basins (Codilean et al., 2021) plus a regional database with 14 basins measured with the same method were used (Mohr et al., 2023). In contrast to denudation rate derived from sediment and solutes fluvial discharge, this method has minimal human disturbance and captures large, infrequent events (Kirchner et al., 2001). To use only reliable average denudation rates, were discarded measurements on sediment higher than 1mm and in basins smaller than 100km^2 or that have lakes area plus their upstream area larger than 25% of the basin surface. The measurements on coarse sediment were removed to avoid variations in ^{10}Be concentration due to grain size and because smaller diameters would better reflect mean denudation rate of all geomorphologic processes taking place in catchments (Carretier et al., 2009; Aguilar et al., 2014). The small basins were filtered to avoid that ^{10}Be concentration does not represent the real denudation rate due to the possible occurrence of landslides with deep-seated failure (Yanites et al., 2009). Finally, the lake basins were discarded because the denudation rate –calculated with spatial information of the whole basin (Codilean et al., 2022)– does not represent the real connected area, i.e., where sediment flux is not trapped by lakes. From the applied filters, 1,708 basins remained, but 15 more were discarded to avoid lose some candidate covariates unavailable for latitudes greater than 60°N (see next section). The 1,693 usable basins have a median integration time of 11.3 kyr and are around all continents except Antarctica (Table S9).

Appendix B: Controlling variables

From several global databases, 47 environmental, candidate covariates were collected or generated. The candidate covariates were divided into the groups Topography, Climate & Vegetation, Seismicity, Lithology and Cryosphere to reduce the computational cost of model building and avoid collinearity (see next section). The first group includes hydrologic variables that are computed with topographic gradient data like stream power, while the second one includes hydrologic variables that are computed without topographic gradient data directly like streamflow and runoff.

Topography

This group contain the variables: area, slope, stream power and Normalized Channel Steepness Index (K_{sn}) using a concavity index equal to 0.4 and 2 thresholds of minimum drainage area (1 and 5 km^2) (Hilley et al., 2019). For the last three variables, in addition to the full averages, the 85th and 95th quantiles were calculated because steep hillslopes erode exponentially more than flat ones (Roering, 2008), and using the average could attenuate this signal. Also, fluvial erosion occurs above a bed shear stress threshold, so low values of stream power and K_{sn} are irrelevant (DiBiase and Whipple, 2011).

The stream power of each river reach in the basins was calculated according to the following formula:

https://doi.org/10.5194/esd-2024-27
Preprint. Discussion started: 23 September 2024

Earth System Dynamics
Discussions
Open Access

$$\omega = \frac{\rho\, g\, Q\, S}{b} \quad (4)$$

where ω is the stream power (W m^{-2}), ρ is the density of water (1,000 kg m^{-3}), g is the acceleration due to gravity (9.8 m s^{-2}), Q is the maximum monthly average streamflow (m^3 s^{-1}), S is the slope (m m^{-1}) and b is the channel width for bankfull stage (m) that was estimated based on Q values and hydraulic geometry laws. River reaches vary in length (average 4km), but were rasterized to 250m before calculating stream power. The river network and the remaining data for each river reach were downloaded from https://www.hydrosheds.org/. In this dataset, it is assumed that a river is generated when catchment area is at least 10 km^2 or average streamflow is at least 0.1 m^3 s^{-1}.

While the slope was calculated with a spatial resolution of 3 arc-second (Lehner et al., 2008), stream power and K_{sn} were calculated with a resolution of 15 arc-second. To ensure that the selection of slope over the other variables was due to natural causes (Discussion section), the calculated slope was replaced by another with a spatial resolution of 15 arc-second, which was also the topographic variable selected with a 1% decrease in model predictability (Table S5).

Climate & vegetation

As climatic variables were obtained present-day average annual precipitation (Zomer et al., 2022), 3 extreme precipitation variables (Beck, et al., 2020; Bezak et al., 2022), 2 soil moisture variables (Guevara et al., 2021), and the aridity index (AI) that is calculated by dividing precipitation with potential evapotranspiration (Zomer et al., 2022). Also was recovered average annual precipitation for the last 11.7kyr (Fordham et al., 2017), which is approximately the median integration time of the denudation rates (Table S9). Regarding hydro-climatic variables, average annual streamflow and maximum monthly average streamflow were obtained (m^3 s^{-1}) (Döll et al., 2003). In turn, these were divided by basins area to obtain runoff values (mm yr^{-1}).

As biologic variables it was obtained the Leaf Area index (Mao and Yan, 2019), 2 estimates of forest cover fraction (Bicheron et al., 2011; Shimada et al., 2014), the average Normalized Difference Vegetation Index (NDVI) (Leon-Tavares et al., 2021) and the C-factor, which indicates land susceptibility to be eroded by runoff (Renard et al., 1997; Borselli et al., 2008) and was calculated from the land cover map of Bicheron et al., (2011) (Table S8). Finally, the first Principal Component of the variables NDVI, AI and paleo-precipitation was calculated to have a variable that summarizes bioclimatic condition. The Principal Component captured 83% of the total variance, in fact, if in the model of Eq. 2 *clim* is replaced by any of the variables that make it up, the positive effect is maintained (Table S14).

Seismicity

For each basin and from Giardini et al., (2003) it was recovered the average peak ground acceleration (PGA; express in m s^{-2}) for a 10% probability of exceedance in 50yr, corresponding to a return period of 475yr. Also, from Pagani et al., (2020) it was obtained the average PGA express in *g* for return periods of 475 and 2,475 yr inferred from topography and not.

Lithology

To estimate lithologic effect, it was used the geologic map of Hartmann and Moosdorf (2012) with an average spatial scale of 1:3,750,000. Following the method proposed by

https://doi.org/10.5194/esd-2024-27
Preprint. Discussion started: 23 September 2024

Earth System Dynamics
Discussions
Open Access

Campforts et al., (2020), to each geologic unit it was assigned an erodibility index between 2 and 12 based on its composition (Table S16). This erodibility index has a well relationship with uniaxial compressive strength at a regional dimension. In this research, values of non-igneous rocks were not weighted by their age as this data was unavailable.

The percentage of each basin with hard lithologies (metamorphic, plutonic and volcanic) and physically or chemically weak lithologies (unconsolidated sediment, evaporites, and pyroclastic and carbonate sedimentary rocks) was also calculated.

Cryosphere

Mean snow water equivalent (SWE; mm yr^{-1}), snow cover days (No. yr^{-1}) and frost change frequency (No. yr^{-1}) for each basin were obtained from Brun et al., (2022). Frost change frequency was used to represent periglacial processes such as frost-cracking. Furthermore, from Millan et al., (2022) average basal velocity (m yr^{-1}) of every glacier in each basin was extracted. With this dataset, the accumulated velocity of each glacier was calculated by multiplying its average velocity with its area. Then, the accumulated velocities of all glaciers in each basin were added and these values were divided by basin area. Compared to glacier area or volume, basal velocity better reflects erosion and can therefore provide more information about the ^{10}Be-depleted sediment mass exported by glaciers (Herman et al., 2021). Finally, the first Principal Component between the four recovered variables was calculated to obtain a one that encompasses all the cryospheric processes involved in ^{10}Be concentration.

Appendix C: Statistical approach

Once the dependent variable and the candidate covariates were collected, the environmental control on denudation rate was analysed using General Linear Model (Anderson et al., 2015). To respect linearity and homoscedasticity assumptions of this statistical method, for variables with skewness greater (less) than 0.5 (-0.5) their natural logarithms were calculated and, if necessary, translations were also be applied (by adding or subtracting a constant) so that they have a normal distribution. An automatic model selection was then performed, in which all possible models were generated by combining the candidate covariates, and the best was selected based on the Akaike Information Criterion (AIC) (Akaike, 1974), which optimises the trade-off between model prediction and complexity, i.e., variables number. To reduce computational cost of this analysis, for candidate covariates of a same group with correlations ≥0.95, those that were not the one with the highest correlation with the dependent variable were removed. Based on this rule, 30 candidate covariates were evaluated for the model building (Table S12). Here, the model selection had the restrictions of: a) for variables belonging to the same group, e.g., Cryosphere, only one could be selected to avoid collinearity and reduce computational cost, and b) the chosen regression had to be physically plausible, e.g., seismicity cannot decrease denudation. The only exception to point a) was the Topography group, where the area was not mutually exclusive with the slope variables, as they represent completely different processes. Once the best model was selected, its AIC was compared with that of another identical model, but which included a multiplication between the topographic and bioclimatic covariates, to know whether the inclusion of the interaction provided a significant improvement (Nelder, 1977).

The coefficient of determination (R^2) of a multiple regression increases when more covariates are introduced regardless of whether there is a real model improvement. So, predictability of the selected model was evaluated through the Adjusted R^2, which is independent of covariates number and therefore is a more robust metric for comparing

https://doi.org/10.5194/esd-2024-27
Preprint. Discussion started: 23 September 2024

multiple regressions. In total, 7,543 multiple regression models were compared (Table S14). The prediction of basins slope was also performed with an automatic model selection (Sup. Material).

References

Aguilar, G., et al., 2014. Grain size-dependent ^{10}Be concentrations in alluvial stream sediment of the Huasco Valley, a semi-arid Andes region. *Quaternary Geochronology*, 19, 163–172. https://doi.org/10.1016/j.quageo.2013.01.011

Akaike, H., 1974. A new look at the statistical model identification. *IEEE Trans. Autom. Control*, 19, 716– 723. https://doi.org/10.1109/TAC.1974.1100705

Amundson, R., Heimsath, A., Owen, J., Yoo, K., Dietrich, W. E. 2015. Hillslope soils and vegetation. *Geomorphology*, 234, 122–132. https://doi.org/10.1016/j.geomorph.2014.12.031

Anderson, D. R, Sweeney, D. J., Williams, T.A. (Eds). 2015. Statistics for Business & Economics. Cengage Learning. ISBN: 978-1-305-58531-7

Antinao, J. L. Gosse, J. 2009. Large rockslides in the Southern Central Andes of Chile (32-34.5°S): Tectonic control and significance for Quaternary landscape evolution. *Geomorphology*, *104*(3–4), 117–133. https://doi.org/10.1016/j.geomorph.2008.08.008

Barnhart, K. R., et al., 2020. Inverting Topography for Landscape Evolution Model Process Representation: 1. Conceptualization and Sensitivity Analysis. *J. Geophys. Res. Earth Surf.*, 125(7). https://doi.org/10.1029/2018JF004961

Beck, H. E., et al., 2020. PPDIST, global 0.1° daily and 3-hourly precipitation probability distribution climatologies for 1979–2018. *Sci. Data*, 7(1), 1–12. https://doi.org/10.1038/s41597-020-00631-x

Bezak, N., Borrelli, P., Panagos, P. 2022. Exploring the possible role of satellite-based rainfall data in estimating inter- and intra-annual global rainfall erosivity. *Hydrol. Earth Syst. Sci.*, 26(7), 1907–1924. https://doi.org/10.5194/hess-26-1907-2022

Bicheron, P., et al., 2011. Geolocation Assessment of MERIS GlobCover Orthorectified Products. *IEEE Transactions on Geoscience and Remote Sensing*, vol. 49, no. 8, pp. 2972-2982. https://doi.org/10.1109/TGRS.2011.2122337

Borselli, L., Cassi, P., Torri, D. 2008. Prolegomena to sediment and flow connectivity in the landscape: A GIS and field numerical assessment. *Catena*, 75(3), 268–277. https://doi.org/10.1016/j.catena.2008.07.006

Brun, P., Zimmermann, N. E., Hari, C., Pellissier, L., Karger, D. N. 2022. A novel set of global climate-related predictors at kilometre resolution. *EnviDat*. https://doi.org/10.5194/essd-2022-212

Campforts, B., et al., 2020. Parameterization of river incision models requires accounting for environmental heterogeneity: Insights from the tropical Andes. *Earth Surf. Dyn.*, 8(2), 447–470. https://doi.org/10.5194/esurf-8-447-2020

Campforts, B., Shobe, C. M., Overeem, I., Tucker, G. E. 2022. The Art of Landslides: How Stochastic Mass Wasting Shapes Topography and Influences Landscape Dynamics. *J. Geophys. Res. Earth Surf.*, *127*(8). https://doi.org/10.1029/2022JF006745

Carretier, S., Regard, V., Soual, C. 2009. Theoretical cosmogenic nuclide concentration in river bed load clasts: Does it depend on clast size? *Quaternary Geochronology*, 4(2), 108–123. https://doi.org/10.1016/j.quageo.2008.11.004

https://doi.org/10.5194/esd-2024-27
Preprint. Discussion started: 23 September 2024

Earth System Dynamics
Open Access
Discussions

Chen, A., Darbon, J. Ô., Morel, J. M. 2014. Landscape evolution models: A review of their fundamental equations. *Geomorphology*, 219. https://doi.org/10.1016/j.geomorph.2014.04.037

Chen, S.A., Michaelides, K., Richards, D.A., Singer, M.B. 2022. Exploring exogenous controls on short- versus long-term erosion rates globally. *Earth Surf. Dyn.*, 10(6), 1055–1078. https://doi.org/10.5194/esurf-10-1055-2022

Codilean, A. T., et al., 2021. Controls on denudation along the East Australian continental margin. *Earth-Sci. Rev.,* 214. https://doi.org/10.1016/j.earscirev.2021.103543

Codilean, A. T., et al., 2022. OCTOPUS database (v.2). *Earth Syst. Sci. Data*, 14(8), 3695–3713. https://doi.org/10.5194/essd-14-3695-2022

Cuffey, K. M., & Paterson, W. S. B. 2010. Basal Slip in Cuffey, K. M., & Paterson, W. S. B (Ed.) *The physics of glaciers* (4th edition). Burlington, MA: Butterworth-Heinemann.

Delunel, R., van der Beek, P.A., Carcaillet, J., Bourlès, D.L., Valla, P.G. 2010. Frost-cracking control on catchment denudation rates: Insights from in situ produced ^{10}Be concentrations in stream sediments (Ecrins-Pelvoux massif, French Western Alps). *Earth Planet. Sci. Lett.*, 293(1–2), 72–83. https://doi.org/10.1016/j.epsl.2010.02.020

DiBiase, R. A., Whipple, K. X. 2011. The influence of erosion thresholds and runoff variability on the relationships among topography, climate, and erosion rate. *J. Geophys. Res. Earth Surf.*, 116(4), 1–17. https://doi.org/10.1029/2011JF002095

Döll, P., Kaspar, F., Lehner, B. 2003. A global hydrological model for deriving water availability indicators: model tuning and validation. *Journal of Hydrology*, 270, 105-134

Ferrier, K.L., Huppert, K.L., Perron, J.T., 2013. Climatic control of bedrock river incision. *Nature* 496, 206–209. https://doi.org/10.1038/nature11982.

Fischer, et al., 2021. Radioactive waste under conditions of future ice ages. In: Haeberli, W., Whiteman, C. (Eds): *Snow and Ice-Related Hazards, Risks and Disasters* – Updated Second Edition; Elsevier. https://doi.org/10.1016/B978-0-12-817129-5.00005-6

Fordham, D. A., et al., 2017. PaleoView: a tool for generating continuous climate projections spanning the last 21 000 years at regional and global scales. *Ecography*, 40(11), 1348–1358. https://doi.org/10.1111/ecog.03031

Forte, A. M., et al., 2022. Low variability runoff inhibits coupling of climate, tectonics, and topography in the Greater Caucasus. *Earth Planet. Sci. Lett.*, 584. https://doi.org/10.1016/j.epsl.2022.117525

Giardini, D., Grünthal, G., Shedlock, K. M., Zhang, P. 2003. The GSHAP Global Seismic Hazard Map. In: Lee, W., Kanamori, H., Jennings, P., Kisslinger, C. (eds.): *International Handbook of Earthquake & Engineering Seismology*, International Geophysics Series 81 B, Academic Press, Amsterdam, 1233-1239.

Guevara, M., Taufer, M., Vargas, R. 2021. Gap-free global annual soil moisture: 15 km grids for 1991–2018, *Earth Syst. Sci. Data*, 13, 1711–1735, https://doi.org/10.5194/essd-13-1711-2021

Harries, R. M., Aron, F., Kirstein, L. A. 2023. Climate aridity delays morphological response of Andean river valleys to tectonic uplift. *Geomorphology*, 108804. https://doi.org/10.1016/j.geomorph.2023.108804

Hartmann, J., Moosdorf, N. 2012. The new global lithological map database GLiM: A representation of rock properties at the Earth surface. *Geochemistry, Geophysics, Geosystems*, 13(12), 1–37. https://doi.org/10.1029/2012GC004370

Heimsath, A.M., Dietrich, W.E., Nishiizumi, K., Finkel, R.C. 1997. The soil production function and landscape equilibrium. *Nature*, 388, 358–361. https://doi.org/10.1038/41056

https://doi.org/10.5194/esd-2024-27
Preprint. Discussion started: 23 September 2024

Herman, F., De Doncker, F., Delaney, I., Prasicek, G., Koppes, M. 2021. The impact of glaciers on mountain erosion. *Nat. Rev. Earth Environ.*, 2(6), 422–435. https://doi.org/10.1038/s43017-021-00165-9

Hilley, G. E., et al., 2019. Earth's topographic relief potentially limited by an upper bound on channel steepness. *Nat. Geosci.*, 12(10), 828–832. https://doi.org/10.1038/s41561-019-0442-3

Hinderer, M., Kastowski, M., Kamelger, A., Bartolini, C., Schlunegger, F. 2013. River loads and modern denudation of the Alps - A review. *Earth-Sci. Rev.*, 118, 11–44. https://doi.org/10.1016/j.earscirev.2013.01.001

Hu, J., Liu, L., Gurnis, M. 2021. Southward expanding plate coupling due to variation in sediment subduction as a cause of Andean growth. *Nat. Commun.*, 12(1), 1–9. https://doi.org/10.1038/s41467-021-27518-8

Iverson, N. R. 2012. A theory of glacial quarrying for landscape evolution models. *Geology*, 40(8), 679– 682. https://doi.org/10.1130/G33079.1

Kirchner, J. W., et al., 2001. Mountain erosion over 10 yr, 10 k.y., and 10 m.y. time scales. *Geology* 7. https://doi.org/10.1130/0091-7613(2001)029<0591:MEOYKY>2.0.CO;2

Koppes, M., et al., 2015. Observed latitudinal variations in erosion as a function of glacier dynamics. *Nature*, 526(7571), 100–103. https://doi.org/10.1038/nature15385

Langbein, W. B., Schumm, S. A. 1958. Yield of sediment in relation to mean annual precipitation, *Eos, Trans. AGU*, 39, 1076–1084, https://doi.org/10.1029/TR039i006p01076

Lehner, B., Verdin, K., Jarvis, A. 2008. New global hydrography derived from spaceborne elevation data. *Eos*, 89(10): 93–94. https://doi.org/10.1029/2008eo100001

Leon-Tavares, J. et al., 2021. Correction of Directional Effects in VEGETATION NDVI Time-Series. *Remote Sens.*, 13(6). https://doi.org/10.3390/rs13061130

Li, D., et al., 2022. High Mountain Asia hydropower systems threatened by climate-driven landscape instability. *Nat. Geosci.* https://doi.org/10.1038/s41561-022-00953-y

Mao, J., B. Yan. 2019. Global Monthly Mean Leaf Area Index Climatology, 1981-2015. ORNL DAAC, Oak Ridge, Tennessee, USA. https://doi.org/10.3334/ORNLDAAC/1653

Marder, E., Gallen, S. F. 2023. Climate control on the relationship between erosion rate and fluvial topography. *Geology,* 51 (5): 424–427. https://doi.org/10.1130/G50832.1

Masotti, I., et al., 2018. The influence of river discharge on nutrient export and phytoplankton biomass off the Central Chile Coast (33°-37°S): Seasonal cycle and interannual variability. *Frontiers in Marine Science*, 5(NOV), 1–12. https://doi.org/10.3389/fmars.2018.00423

Millan, R., Mouginot, J., Rabatel, A., Morlighem, M. 2022. Ice velocity and thickness of the world's glaciers. *Nat. Geosci.*, 15(2), 124–129. https://doi.org/10.1038/s41561-021-00885-z

Mishra, A. K., Placzek, C., Jones, R. 2019. Coupled influence of precipitation and vegetation on millennial-scale erosion rates derived from ^{10}Be, *PloS One*, 14, e0211325, https://doi.org/10.1371/journal.pone.0211325

Mohr, C., et al., 2023. Dense vegetation promotes denudation in Patagonian rainforests. *Authorea*, 1–40. 10.1002/essoar.10511846.1

Murphy, B. P., Johnson, J. P. L., Gasparini, N. M., Sklar, L. S. 2016. Chemical weathering as a mechanism for the climatic control of bedrock river incision. *Nature*, *532*(7598), 223–227. https://doi.org/10.1038/nature17449

Nelder, J. A. 1977. A Reformulation of Linear Models. *Journal of the Royal Statistical Society*, 140(1), 48- 77. https://doi.org/10.2307/2344517

Pagani, M. et al., 2020. The 2018 version of the Global Earthquake Model: hazard component. *Earthq. Spectra.* https://doi.org/10.1177/8755293020931866

Perron, J.T. 2017. Climate and the Pace of Erosional Landscape Evolution. *Annu. Rev. Earth Planet. Sci.*, 45, 561–591. https://doi.org/10.1146/annurev-earth-060614-105405

Porder, S. 2019. How Plants Enhance Weathering and How Weathering is Important to Plants. *Elements*, 15(4), 241–246. https://doi.org/10.2138/gselements.15.4.241

Portenga, E.W., Bierman, P.R. 2011. Understanding earth's eroding surface with ^{10}Be. *GSA Today*, 21(8), 4–10. https://doi.org/10.1130/G111A.1

Rehak, K., Bookhagen, B., Strecker, M. R., Echtler, H. P. 2010. The topographic imprint of a transient climate episode: The western Andean flank between 15·5° and 41·5°S. *Earth Surf. Process. Landf.*, *35*(13), 1516–1534. https://doi.org/10.1002/esp.1992

Renard, K., Foster, G.R., Weessies, G.A., Mc Cool, D.K., Yodler, D.C., 1997. Predicting soil erosion by water— a guide to conservation planning with the Revised Universal Soil Loss Equation (RUSLE). U.S. D.A.- A.R.S., Handbook No 703. 384 pp. https://handle.nal.usda.gov/10113/11126

Riebe, C.S., Granger, D.E. 2013. Quantifying effects of deep and near-surface chemical erosion on cosmogenic nuclides in soils, saprolite, and sediment. *Earth Surf. Process. Landf.*, *38*(5), 523–533. https://doi.org/10.1002/esp.3339

Roering, J. 2008. How well can hillslope evolution models "explain" topography? Simulating soil transport and production with high-resolution topographic data. *Geol. Soc. Am. Bull.*, *120*(9–10), 1248–1262. https://doi.org/10.1130/B26283.1

Roering, J. Landslides limit mountain relief. *Nat. Geosci.*, 5, 446–447 (2012). https://doi.org/10.1038/ngeo1511

Ruetenik, G., Jansen, J. D., Val, P., and Ylä-Mella, L. 2023 Optimising global landscape evolution models with ^{10}Be, *Earth Surf. Dynam*. https://doi.org/10.5194/esurf-11-865-2023

Schmid, M., Ehlers, T.A., Werner, C., Hickler, T., Fuentes-Espoz, J.P. 2018. Effect of changing vegetation and precipitation on denudation - Part 2: Predicted landscape response to transient climate and vegetation cover over millennial to million-year timescales. *Earth Surf. Dyn.*, 6(4), 859–881. https://doi.org/10.5194/esurf-6-859-2018

Seybold, H., Berghuijs, W. R., Prancevic, J. P., Kirchner, J. W. 2021. Global dominance of tectonics over climate in shaping river longitudinal profiles. *Nat. Geosci.*, 14(7), 503–507. https://doi.org/10.1038/s41561-021-00720-5

Shimada, M., et al., 2014. New global forest/non-forest maps from ALOS PALSAR data (2007-2010). *Remote Sens. Environ.*, 155, 13–31. https://doi.org/10.1016/j.rse.2014.04.014

Smith, A. G. G., Fox, M., Schwanghart, W., Carter, A. 2022. Comparing methods for calculating channel steepness index. *Earth-Sci. Rev.*, 227(103970). https://doi.org/10.1016/j.earscirev.2022.103970

Torres Acosta, V., et al., 2015. Effect of vegetation cover on millennial-scale landscape denudation rates in East Africa. *Lithosphere*, 7(4), 408–420. https://doi.org/10.1130/L402.1

Vergani, C., et al., 2017. Root reinforcement dynamics of European coppice woodlands and their effect on shallow landslides: A review, *Earth-Sci. Rev.*, 167, 88–102, https://doi.org/10.1016/j.earscirev.2017.02.002

Vergara I, Garreaud R, Araneo D, Leyton F. 2023 Environmental control of the present-day sediment export along the extratropical Andes. *Geomorphology*. 441:1-9. https://doi.org/10.1016/j.geomorph.2023.108911

https://doi.org/10.5194/esd-2024-27
Preprint. Discussion started: 23 September 2024

Earth System Dynamics
Discussions

Vergara I, Garreaud R, Ayala Á. 2022. Sharp increase of extreme turbidity events due to deglaciation in the subtropical Andes. *J. Geophys. Res. Earth Surf.* 10.1029/2021JF006584

Vergara, I., Moreiras, S. M., Santibañez, F., Araneo, D., Ferrando, F. 2020. Debris flows triggered from melt of seasonal snow and ice within the active layer in the semi-arid Andes. *Permafr. Periglac. Process.*, 31(1), 57–68. https://doi.org/10.1002/ppp.2020

Walling, D., Kleo, A. H. A. 1979. Sediment yields of rivers in areas of low precipitation: a global view, in: *The Hydrology of Areas of Low Precipitation*, IAHS Publications, Wallingford, Oxfordshire, UK, 128, 479–493

West, J. A. 2012. Thickness of the chemical weathering zone and implications for erosional and climatic drivers of weathering and for carbon-cycle feedbacks. *Geology*, *40*(9), 811–814. https://doi.org/10.1130/G33041.1

Whipple, K.X., 2009. The influence of climate on the tectonic evolution of mountain belts. *Nat. Geosci.*, 2, 97–104. https://doi.org/10.1038/ngeo413

Willenbring, J. K., Codilean, A. T., McElroy, B. 2013. Earth is (mostly) flat: Apportionment of the flux of continental sediment over millennial time scales. *Geology*, 41(3), 343–346. https://doi.org/10.1130/G33918.1

Yanites, B. J., Tucker, G. E., Anderson, R. S. 2009. Numerical and analytical models of cosmogenic radionuclide dynamics in landslide-dominated drainage basins. *J Geophys. Res. Earth Surf.*, 114(1). https://doi.org/10.1029/2008JF001088

Zhang, T., et al., 2022. Warming-driven erosion and sediment transport in cold regions. *Nat. Rev. Earth Environ.* https://doi.org/10.1038/s43017-022-00362-0

Zomer, R. J., Xu, J., Trabucco, A. 2022. Version 3 of the Global Aridity Index and Potential Evapotranspiration Database. *Sci. Data*, 9(1), 1–15. https://doi.org/10.1038/s41597-022-01493-1

Data availability: All databases used are publicly accessible and their repositories are cited throughout the manuscript and the Supplementary Material. No specific codes were generated. Model selection and graphical representation of covariates effects were performed using the *MuMIn* and *effects* packages of the RStudio software, respectively.

Author Contributions: I. V. designed the study. I. V. and F. S. conducted the analyses. All authors interpreted the analyses and contributed to the paper writing.

Competing interests: The authors declare no competing interests.

Acknowledgments: I. V. and R. G. are partially supported by CR2 - FONDAP/ANID 1522A0001.